Comparative Analysis of Single-Star and Dual-Star Permanent-Magnet Synchronous Machines

A. Abedini Mohammadi, S. Ciceo, Y. Mollet, A-C Pop, and J. Gyselinck, *IEEE memeber*

***Abstract*—The performance of a fractional-slot concentrated-winding PMSM with two different winding diagrams, namely, single and dual star, is investigated. Firstly, the air-gap flux density for these two cases in terms of rotating fields is studied, which provides insight into the essential difference between these two windings. Then, a computationally efficient model taking into account saturation and spatial effects using FE-obtained look-up tables is developed. Using the model, the control and the offline design of the controllers are carried out based on the two-axis reference frame model for both machines and the vector space decomposition for dual-star one. The comparison is made in terms of terminal current harmonics, torque ripple, power density, and closed-loop control dynamic performance. It is shown that the dual-star machine has higher power density and less torque ripple, but higher 5th and 7th current harmonics. Moreover, the effect of one imperfection which may come with the dual-star winding diagram, namely imperfect electrical phase shift between the respective currents or voltages of two stars, on the performance of the machine is studied. It is concluded that the imperfection can deteriorate the closed-loop dynamic performance.**

***Index Terms*—dual-star winding, permanent-magnet synchronous machine, space vector decomposition, vector control**

I. Introduction

Permanent-magnet synchronous machines (PMSMs) are widely used in the automotive industry [1]. They have the highest power/torque density among commercial electrical machines and can have similar dynamic performance to conventional brushed DC machines but with less maintenance [2]. They are commercialized for the various applications in cars, including auxiliary applications like electric power steering systems [3] or traction motor for the powertrain [4].

However, automotive applications demand for further requirements including high reliability and fault-tolerance capability. In general, PMSM drives are subject to multiple faults on both converter and machine sides. The most common faults are open-circuits and short-circuits in the inverter switches, which make one or several phases out of operation [5]. Even upon occurrence of a fault, PMSMs should be able to provide the required output torque with acceptable ripple for a certain time.

A winding scheme consisting of multiple phases (more than three) is a common solution for having a fault-tolerant electric drive [6], [7]. A higher number of phases provides more possibilities for efficient control methods in the case of a fault. Moreover, these machines can have higher power density, and less torque ripple. However, these advantages come with some drawbacks, namely higher current harmonics and possible electromagnetic imbalance between the stars for multi-star winding diagrams.

Dual-star winding otherwise known as asymmetrical 6-phase winding is a proved diagram for PMSMs. The winding consists of two stars shifted from each other by 30 electrical degrees and the neutral points are galvanically isolated. This winding diagram is known for high value of fifth and seventh current harmonics [8], [9].

This paper makes a comparison between two equivalent PMSMs: one single star (SiSPMSM) and dual-star one (DuSPMSM). A commercially available rewound concentrated-winding power-steering 3-phase machine is selected for the study and the equivalent dual-star machine is derived by simply changing coil connections. The airgap flux density of these machines is investigated in terms of rotating fields. Then, the overall performance of the machines is compared in terms of phase-current harmonics, torque ripple, dynamic performance, and power density.

Detailed models of the machines are developed using FE-obtained look-up tables (LUTs), which allow considering current and torque harmonics produced by saturation and spatial effects with good accuracy. Then, the control structure and the offline design of the controllers are done in dq reference frame. Moreover, vector space decomposition (VSD) transformation is applied for the control of DuSPMSM.

Moreover, the effect of imperfect phase shift between the currents or voltages of the two stars which may exist in dual-star drives with two separate inverters is studied [10]. It can be due to unsynchronized processors used by the two inverters for producing PWM signals. Because of this defect, there can be a phase shift different from 30 electrical degrees between the respective voltages of the two stars.

II. The machine under study

The machine under study is a 12/10 interior-PMSM, i.e. 12 stator teeth and 10 poles, with concentrated winding. The

This paper is part of the European Industrial Doctorate on Next Generation for sustaINable auTomotive ElectRical ACtuaTion (INTERACT) project which has received funding from the European Union Horizon 2020 research and innovation programme under grant agreement No 766180.

A. Abedini Mohammadi, S. Ciceo, Y. Mollet, and J. Gyselinck are with BEAMS Department, Electrical Energy Group, Université libre de Bruxelles, Brussels, Belgium

A. Abedini Mohammadi and A-C Pop are with Brose Fahrzeugteile SE & Co. KG, Würzburg, Germany

S. Ciceo and Y. Mollet are with Engineering Services RTD, & TEST MBST Departments Siemens Industry Software NV, Leuven, Belgium

S. Ciceo is with Department of Electrical Machines and Drives, Technical University of Cluj-Napoca, Cluj-Napoca, Romania

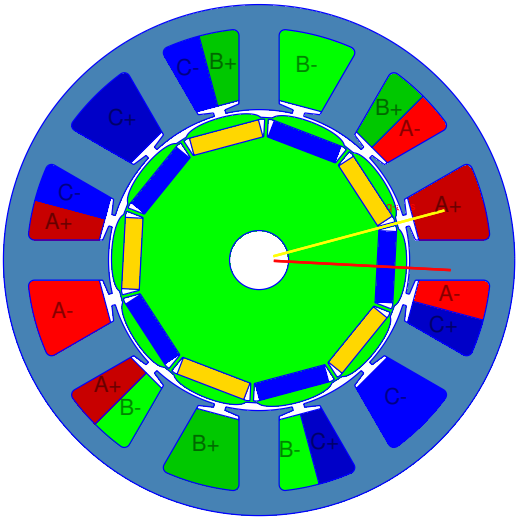

Fig. 1. Cross-section of the original SiSPMSM

specifications of the rewound SiSPMSM are reported in Table I. The cross-section of the machine along with coil side connections are illustrated in Fig 1. Each coil has 125 turns and there are two series coils per phase with two parallel paths. The stator of the rewound machine is shown in Fig. 2. Simply by splitting the two adjacent series coils in each phase into two phases the equivalent dual-star machine is obtained. The current rating of each phase is the same as the original one. However, the nominal voltage of each star decreases by half, as the number of series turns per phase is half of the original machine.

The original machine is designed for electrical power assisted steering system. However, for the sake of bench implementation, the machine has been rewound to increase the nominal voltage from 4 to 62.5 V(RMS) and to decrease the nominal currents from 110 to 7 A(RMS). Keeping the same ampere-turn per slot, the overall performance of the machine remains intact. A picture of rewound stator is given in 2.

III. Airgap Flux density

The interaction between the armature magneto-motive force with the airgap flux density is traditionally used for

TABLE I
SPECIFICATIONS OF THE REWOUND SiSPMSM

Power	800 W
Base speed	1000 rpm
Maximum speed	3600 rpm
Nominal current (RMS)	7 A
Phase voltage (RMS)	62.5 V
Number of turns per coil	125
Stator and rotor iron	M330-50A
Magnet remnant field	1.35 T
Minimum air gap	0.55 mm
PM thickness	3 mm
Stack length	57 mm
Outer dia. of stator	86.6 mm
Outer dia. of rotor	50 mm
Fill factor	38 %

Fig. 2. Stator of the rewound machine

describing the torque generation mechanism in electrical machines. The air gap flux density is a periodical function of the position in the airgap and time. Therefore, it can be decomposed into components known as rotating fields via the 2D Fourier series. The radial component of the airgap flux density, e.g. in the middle of airgap, can be represented as:

$$B_{\mathrm{r}}(\theta,t)=\sum_{n=1}^{\infty}\sum_{m=-\infty}^{\infty}B_{n,m}\cos(2\pi nft-mh\theta+\varphi_{n,m}) \quad (1)$$

where n and m are temporal and spatial orders of the harmonic, and $B_{n,m}$ and $\varphi_{m,n}$ its amplitude and phase, resp. h is the greatest common divisor of number of pole pairs, p, and number of stator slots, N_s, and f the electrical frequency of rotor speed. Positive spatial order means clockwise rotating field and negative spatial order counter-clockwise rotating field (the direction of rotor rotation).

Based on the above equation, the airgap flux density due to the PMs and armature currents for both winding diagrams are shown in Fig. 3. 3.6 k samples over one spatial period, 360 mechanical degree, and 72 samples over one temporal period is considered. Moreover, the winding is fed with purely sinusoidal, balanced currents.

In the first figure, the rotating fields only due to the PMs are shown. The main harmonic responsible for the torque generation is of spatial order -5 and temporal order 1 and has the highest amplitude. There are also rotating fields with orders $(-p(2k-1),2k-1)$, where the first number is spatial order and the second number temporal one, and k a positive integer number. Moreover, due to the stator slots and rotor saliency, harmonics with order $(-p(2t-1)\pm 12k, 2t-1)$ are present, where t and $k\in\{1,2,..\}$.

The second figure shows the rotating fields only due to the armature reaction of the SiSPMSM with the balanced currents. Along side with main harmonic, there are harmonics with order $(-5\pm 6k, 1)$ which are due to the non-sinusoidal distribution of the winding. As the currents are purely sinusoidal, all of these harmonics have the same temporal order. Moreover, the harmonics with order $(-p(2t-1)\pm 6k, 2t-1)$ are present, where t and $k\in\{1,2,..\}$; these harmonics are due to the stator slots and rotor magnetic saliency. As it can be seen in Fig. 3 (c), The orders of the radial magnetic flux

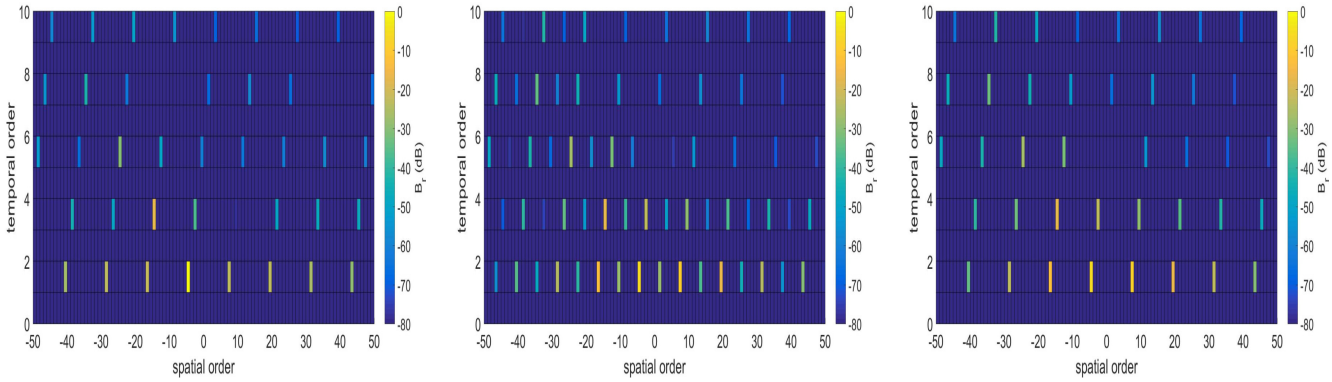

(a) PMs (b) Armature reaction of SiSPMSM (c) Armature reaction of DuSPMSM

Fig. 3. decomposing of the radial magnetic flux density in the middle of the air gap into rotating field due to the (a) PMs, (b) armature reaction of SiSPMSM, and (c) armature reaction of DuSPMSM ($20\text{dB} = 20\log_{10}(10)$)

density due to the winding currents with dual-star winding are the same as that of PMs.

The interaction between the rotating fields due to PMs and the stator winding results in DC or pulsating torque. The relative speed of the rotating fields determiners the frequency of the resulting torque. Therefore, the interaction of the harmonics with same order results in DC torque and contributes to the average torque. The harmonics with different spatial orders are orthogonal and do not contribute to the output torque, while the harmonics with same spatial orders (regardless of rotation sense) and different temporal orders results in pulsating torque.

Two important conclusions can be drawn from the harmonic content of the airgap flux density. In the dual star machine, as there are no harmonics with spatial orders $-p(t \pm 6k)$, k and $t \in \{1, 3, ..\}$, torque harmonics which are odd multiples of 6 do not produce. On the other hand, because of flux density harmonics of PM with orders $(-p(6k-1), 6k-1)$, $k \in \{2, 3, ..\}$, the voltage harmonics with the same temporal orders are induced in the stator phases. These harmonics result in current harmonics with the same temporal orders as their producing voltages. However, as the flux density harmonics due to armature reaction with spatial orders $(-pt \pm 6k)$ cannot enter the airgap, these current harmonics will be only limited by the slot leakage inductance. As a result, corresponding current harmonics can have relatively large amplitude.

The flux density harmonic contents shown in Fig. 3 (a) and (b) are obtained with the same q-axis currents and zero d-axis currents for SiSPMSM and DuSPMSM. The amplitude of the main flux density components, i.e. order (5,1), in the SiSPMSM and DuSPMSM are 0.44 T and 0.456 T, respectively. It shows that for the same current amplitude, DuSPMSM can achieve higher flux density and consequently higher output torque.

IV. Model of the PMSMs

FE-obtained models using LUTs are used for the modelling of the machines [11], [12]. Ignoring eddy currents and iron losses, the relation between d- and q-axis flux linkages and currents along with rotor position dependence are obtained via a series of magnetostatic FE calculations and saved in LUTs:

$$\psi_x(i_{\mathrm{d1}}, i_{\mathrm{q1}}, i_{\mathrm{d2}}, i_{\mathrm{q2}}, \theta_r), x \in \{\mathrm{d1}, \mathrm{q1}, \mathrm{d2}, \mathrm{q2}\} \quad (2)$$

where Ψ_x and i_x are flux linkage and currents of corresponding axis and θ_r the rotor position. For the single-star machine only star 1 values are relevant. The open-source software GetDP/Gmsh is used for the FE modelling. Then, using flux linkage-based state-space equations the transient model of the machine can be implemented either with Park or VSD transformations [4], [13]. The governing equations in dq reference frame are:

$$v_{\mathrm{d1}} = r i_{\mathrm{d1}} + \frac{\mathrm{d}\psi_{\mathrm{d1}}}{\mathrm{d}t} - \omega_r \psi_{\mathrm{q1}} \quad (3)$$

$$v_{\mathrm{q1}} = r i_{\mathrm{q1}} + \frac{\mathrm{d}\psi_{\mathrm{q1}}}{\mathrm{d}t} + \omega_r \psi_{\mathrm{d1}} \quad (4)$$

$$v_{\mathrm{d2}} = r i_{\mathrm{d2}} + \frac{\mathrm{d}\psi_{\mathrm{d2}}}{\mathrm{d}t} - \omega_r \psi_{\mathrm{q2}} \quad (5)$$

$$v_{\mathrm{q2}} = r i_{\mathrm{q2}} + \frac{\mathrm{d}\psi_{\mathrm{q2}}}{\mathrm{d}t} + \omega_r \psi_{\mathrm{d2}} \quad (6)$$

where v_x is the voltage with $x \in \{\mathrm{d1}, \mathrm{q1}, \mathrm{d2}, \mathrm{q2}\}$, r the resistance of each phase, assumed to be the same for all phases, and ω_r the synchronous speed (in electrical rad/sec). For the single star machine only equations related to the first star, i.e. (3) and (4), are relevant and the flux linkages are only a function of star 1 currents. Because of mutual flux linkage between the phases of the two stars, there is relatively strong coupling between d and q axes flux linkages. The corresponding equations with VSD transformation are [13]:

$$v_{\mathrm{D}} = r i_{\mathrm{D}} + \frac{\mathrm{d}\psi_{\mathrm{D}}}{\mathrm{d}t} - \omega_r \psi_{\mathrm{Q}} \quad (7)$$

$$v_{\mathrm{Q}} = r i_{\mathrm{Q}} + \frac{\mathrm{d}\psi_{\mathrm{Q}}}{\mathrm{d}t} + \omega_r \psi_{\mathrm{D}} \quad (8)$$

$$v_{\mathrm{z1}} = r i_{\mathrm{z1}} + \frac{\mathrm{d}\psi_{\mathrm{z1}}}{\mathrm{d}t} - \omega_r \psi_{\mathrm{z2}} \quad (9)$$

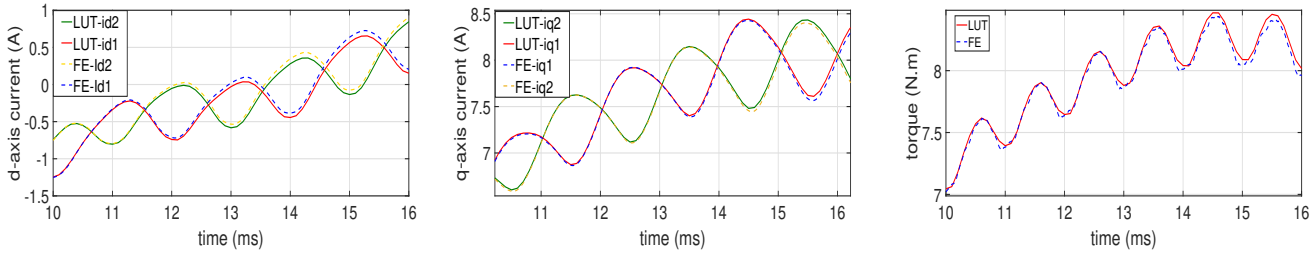

(a) d-axis currents (b) q-axis current (c) Torque

Fig. 4. Part of transient response with imposed step voltages with zero initial values obtained by LUT-based and FE mode at 1000 rpm, (a) d-axis currents, (b) q-axis current, and (c) torque of the dual-star PMSM

$$v_{\mathrm{z2}} = r i_{\mathrm{z2}} + \frac{\mathrm{d}\psi_{\mathrm{z2}}}{\mathrm{d}t} + \omega_r \psi_{\mathrm{z1}} \tag{10}$$

where v_x, i_x, and ψ_x are voltage, current, and flux linkages with $x \in \{\mathrm{D}, \mathrm{Q}, \mathrm{z1}, \mathrm{z2}\}$, respectively. With VSD transformation, both stars are treated as a single winding, and the fundamental and $(12k \pm 1)$th harmonics are transformed to one subspace, DQ, and $(6k \pm 1)th$ harmonics are transformed to another subspace, z1z2. The equations in DQ subspace are like those of a single star machine without explicit coupling.

The relation between the currents obtained by these two transformations are:

$$i_{\mathrm{D}} = \frac{i_{\mathrm{d1}} + i_{\mathrm{d2}}}{2} \text{ and } i_{\mathrm{Q}} = \frac{i_{\mathrm{q1}} + i_{\mathrm{q2}}}{2} \tag{11}$$

$$i_{\mathrm{z1}} = \frac{i_{\mathrm{d2}} - i_{\mathrm{d1}}}{2} \text{ and } i_{\mathrm{z2}} = \frac{i_{\mathrm{q2}} - i_{\mathrm{q1}}}{2} \tag{12}$$

Similar relations are valid for the voltage and flux linkages. Moreover, ignoring the mutual leakage inductance between the two stars, the relation between the inductances are:

$$L_{\mathrm{D}} = L_{\mathrm{d1}} + M_{\mathrm{d1d2}} = L_{\mathrm{d2}} + M_{\mathrm{d2d1}} \tag{13}$$

$$L_{\mathrm{Q}} = L_{\mathrm{q1}} + M_{\mathrm{q1q2}} = L_{\mathrm{q2}} + M_{\mathrm{q2q1}} \tag{14}$$

$$L_{\mathrm{z1}} = L_{\mathrm{d1}} - M_{\mathrm{d1d2}} = L_{\mathrm{d2}} - M_{\mathrm{d2d1}} \tag{15}$$

$$L_{\mathrm{z2}} = L_{\mathrm{q1}} - M_{\mathrm{q1q2}} = L_{\mathrm{q2}} - M_{\mathrm{q2q1}} \tag{16}$$

where L_x and M_{x1x2} are the self- and mutual inductances, respectively. Transient results of d- and q- axis currents along with torque obtained by the LUT-based model and FE for the dual-star machine at 1000 rpm and imposed step voltage with zero initial are shown in Fig. 4, respectively. More details about the LUT-based model are presented in [12].

V. Control of the PMSMs

Both machines are vector controlled. However, two different transformations are used for the design of the controllers of the dual-star machine: Park and VSD transformation.

The control block is made up of 4 PI controllers for the dual-star machine and 2 for the single-star one, see Fig. 5. With the dq model, 4 currents (2 for each star) are controlled separately, while the average value of currents of both stars are controlled in DQ subspace and 5th and 7th current harmonics are controlled in z1z2 subspace. The zero-pole cancellation method is used for designing the controllers. Moreover, feedforward compensation is used for improving dynamic performance. The inductance values used to tune the coefficients of the controllers along with flux linkages for the decoupling network are calculated and updated in each step using LUTs.

VI. Simulation Results

In Fig. 6 to 8, the response to a step in reference currents of both machines and the two control methods are shown with the reference values of $i_{\mathrm{q1}} = i_{\mathrm{q2}} = i_{\mathrm{Q}} = 9A$ and $i_{\mathrm{d1}} = i_{\mathrm{d2}} = i_{\mathrm{D}} = 0A$, at 1000 rpm, and zero initial currents. Moreover, the output torque, closed loop rise time, and current and torque harmonics are reported in Table 2. The cut-off frequency for all of the controllers is the same except for the two controllers in z1z2 subspace. As the currents in z1z2 subspace are pulsating, the cut-off frequency for z1z2 subspace is 6 times of other controllers. The dynamic performance of DuSPMSM with VSD control is the same as SiSPMSM. In fact, with VSD control, the decoupling is accomplished more effectively than with dq control. The torque harmonics of the dual-star machine are a bit higher than those of SiSPMSM. As the machine is designed for power-steering application, it has inherently smooth torque and negligible 6th torque harmonics, and therefore the effect of nullifying 6th torque harmonic by dual-star winding is not noticeable on the overall torque ripple. With given currents, the average torque for the DuSPMSM is higher than SiSPMSM by 4.5%.

Current THDs for the DuSPMSM are higher than SiSPMSM. However, with VSD control method, thanks to the higher cut-off frequency of the controllers in the z1z2 plane, the current harmonics can be reduced to some extent. However, given the limited bandwidth of the controllers in

TABLE II
ELECTRICAL SPECIFICATIONS OF THE SINGLE-STAR PMSM

	SiSPMSM	DuSPMSM (dq, VSD)
Current THD (%)	1.14	4.63, 3.32
6th TH[1] (N.m)	0.015	0, 0
12th TH (N.m)	0.19	0.22, 0.22
Average torque (N.m)	8.8	9.22, 9.15
Rise time (0 to 90%) (ms)	5	7, 5

[1] Torque harmonic

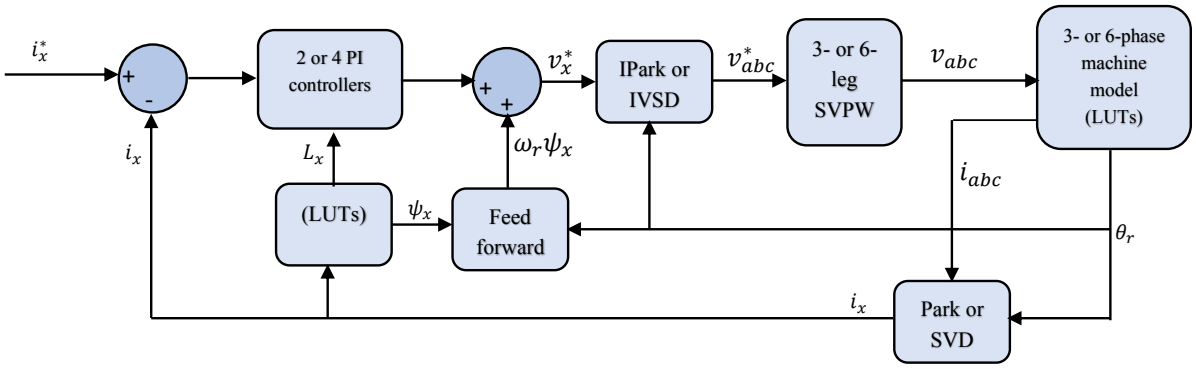

Fig. 5. General control block diagram with Park or VSD transformations and single- or dual-star PMSMs

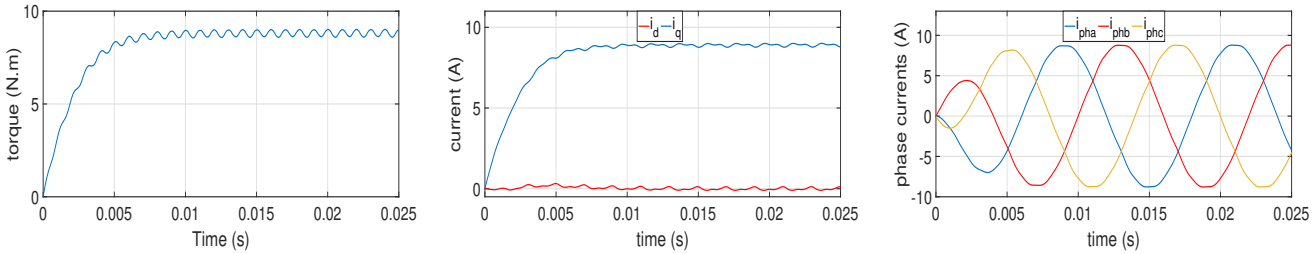

(a) Torque (b) d- and q-axis currents (c) Phase currents

Fig. 6. (a) torque, (b) d- and q-axis currents, and (c) phase currents of SiSPMSM

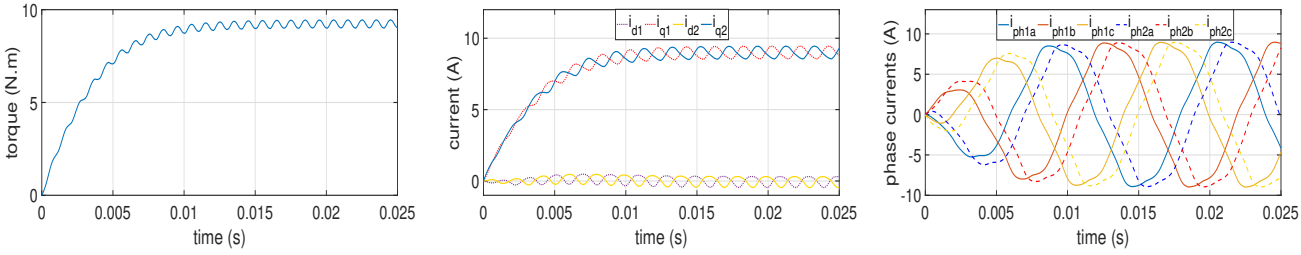

(a) Torque (b) d- and q-axis currents (c) Phase currents

Fig. 7. (a) torque, (b) d- and q-axis currents, and (c) phase currents of DuSPMSM vector-controlled based on dq transformation

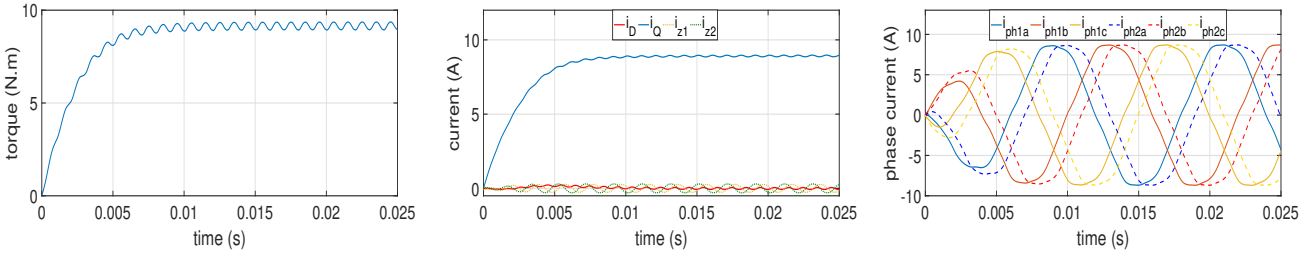

(a) Torque (b) d- and q-axis currents (c) Phase currents

Fig. 8. (a) torque, (b) d- and q-axis currents, and (c) phase currents of DuSPMSM vector-controlled based on VSD transformation

practice, even with VSD-based control the higher THD of current cannot be fully addressed. Moreover, in Fig. 9 the phase current THD and peak-to-peak torque ripple where $i_{\mathrm{q1}} = i_{\mathrm{q2}} = [1:1:9]$A and $i_{\mathrm{d1}} = i_{\mathrm{d2}} = [-5:1:1]$A, for both SiSPMSM and DuSPMSM are shown. It is assumed that the reference currents are the same for both stars and the control is based on dq transformation. Moreover, the results are for given speed of 1000 rpm. It should be mentioned that as both induced voltage and reluctance are proportional to speed, the current THD is not affected by the speed. It can be observed that with negative i_{d}, which is required for the flux weakening, the current THD tends to decrease. the lower

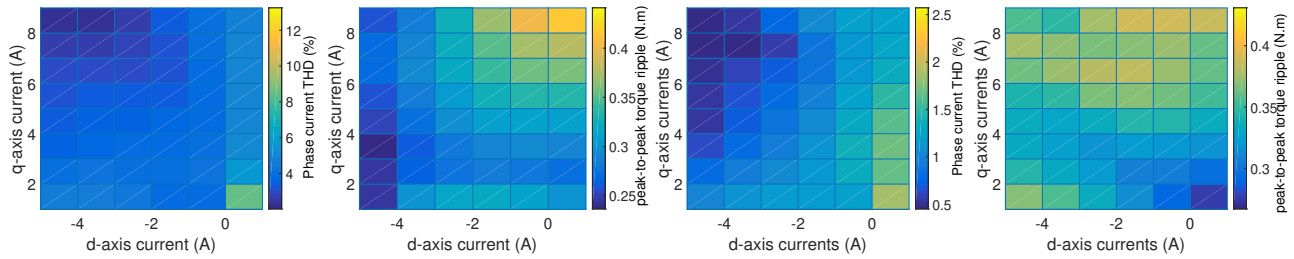

(a) THD of DuSPMSM (b) Torque ripple of DuSPMSM (c) THD of SiSPMSM (d) Torque ripple of SiSPMSM

Fig. 9. THD and torque ripple of SiSPMSM and DuSPMSM with $i_{q1} = i_{q2} = [1:1:9]$A and $i_{d1} = i_{d2} = [-5:1:1]$A

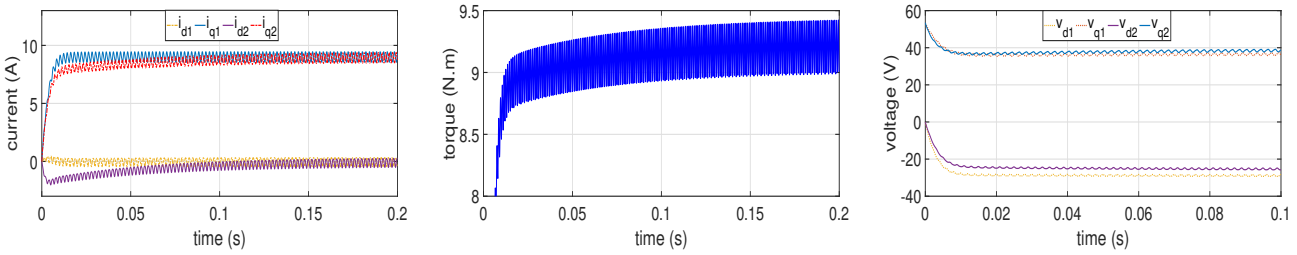

(a) Current (b) Torque (c) Voltage

Fig. 10. (a) current, (b) torque, and (c) voltage of DuSPMSM with imperfect phase shift between voltages of the two stars

current THD can be attributed to lower saturation of the iron and reduced 5th and 7th voltage harmonics. Moreover, the torque ripple with negative i_d for the DuSPMSM is lower than that of SiSPMSM.

Finally, the effect of imperfect phase shift between the voltages of the two stars is investigated. It is assumed that while there is 30 °elec phase shift between the angles of the two transformations used for calculating the reference voltages of the two inverters, the phase shift between the output voltages of the two inverters does not vary with time but is not exactly 30 °elec. The discrepancy depends on switching frequency, pole pairs, and the speed. The higher the speed and pole pair may result in greater disagreement. It can be as big as the electrical angle corresponds to the switching periodicity.

The simulations are done with the machine controlled with the dq transformation. In Fig. 10 the simulation results are shown with the phase shift of 25 °elec. Thanks to the decoupling network, the currents of star 1 is not effected. The closed-loop dynamic performance of star 2 currents is deteriorated. However, after some transient period, the controllers compensate the imperfect phase shift. In fact, with the exact phase shift between the stars, v_{d2} and v_{q2} are equal with the v_{d1} and v_{q1}, respectively. With the imperfect phase shift, however, they are adjusted in such a way that even with the malfunction of the second inverter the currents reach staedy-state values.

VII. Conclusion

In this paper, two equivalent single-star and dual-star PMSMs are compared. Firstly, the fundamental differences between these two winding diagrams are investigated in terms of rotating fields. Then, A FE-based model of the machine is developed which can take into account the harmonics due to saturation and non-sinusoidal distribution of winding into account. The dual-star machine has higher average output torque for given currents and lower torque ripple. However, 5th and 7th current harmonics are relatively high. Moreover, due to the magnetic coupling between the stars, the dynamic performance of the dual-star machine, e.g. response time, is not as fast as that of single-star one. However, with SVD transformation the coupling between stars can be addressed. Moreover, the effect of imperfect phase shift between the two stars are studied and shown the PI controllers are able to compensate this defect. Experimental results will be included in future works.

References

[1] A.-C. Pop, J. J. Gyselinck, D. E. Pinto, and I. Vintiloiu, "Optimization of low-power brushless pm-machines for automotive applications with focus on high-volume mass production," *IEEE transactions on industrial electronics*, vol. 64, no. 12, pp. 9767–9775, 2017.

[2] S. Vaez-Zadeh, *Control of permanent magnet synchronous motors*. Oxford University Press, 2018.

[3] C. Oprea and C. Martis, "Fault tolerant permanent magnet synchronous machine for electric power steering systems," in *2008 International Symposium on Power Electronics, Electrical Drives, Automation and Motion*. IEEE, 2008, pp. 256–261.

[4] P. Hollstegge, D. Keller, and R. W. De Doncker, "Dual three-phase machine modeling and control including saturation, rotor position dependency and reduction of low current harmonics," in *2017 7th International Electric Drives Production Conference (EDPC)*. IEEE, 2017, pp. 1–9.

[5] B. Lu and S. K. Sharma, "A literature review of igbt fault diagnostic and protection methods for power inverters," *IEEE Transactions on Industry Applications*, vol. 45, no. 5, pp. 1770–1777, 2009.

[6] B. Basler, T. Greiner, and P. Heidrich, "Fault-tolerant strategies for double three-phase pmsm used in electronic power steering systems," in *2015 IEEE Transportation Electrification Conference and Expo (ITEC)*. IEEE, 2015, pp. 1–6.
[7] M. Naidu, S. Gopalakrishnan, and T. Nehl, "Fault tolerant permanent magnet motor drive topologies for automotive x-by-wire systems," in *2008 IEEE Industry Applications Society Annual Meeting*. IEEE, 2008, pp. 1–8.
[8] Z. Ruan, W. Song, and Y. Yan, "Current harmonic suppression for dual three-phase permanent magnet synchronous motor drives," *IEEE Access*, vol. 7, pp. 143 888–143 898, 2019.
[9] Y. Hu, Z.-Q. Zhu, and K. Liu, "Current control for dual three-phase permanent magnet synchronous motors accounting for current unbalance and harmonics," *IEEE Journal of Emerging and Selected Topics in Power Electronics*, vol. 2, no. 2, pp. 272–284, 2014.
[10] J. Karttunen, S. Kallio, P. Peltoniemi, P. Silventoinen, and O. Pyrhönen, "Dual three-phase permanent magnet synchronous machine supplied by two independent voltage source inverters," in *International Symposium on Power Electronics Power Electronics, Electrical Drives, Automation and Motion*. IEEE, 2012, pp. 741–747.
[11] D. E. Pinto, A.-C. Pop, J. Kempkes, and et al, "dq0-modeling of interior permanent-magnet synchronous machines for high-fidelity model order reduction," in *2017 International Conference on Optimization of Electrical and Electronic Equipment (OPTIM) & 2017 Intl Aegean Conference on Electrical Machines and Power Electronics (ACEMP)*. IEEE, 2017, pp. 357–363.
[12] A. A. Mohammadi, J. Gyselinck, and A.-C. Pop, "Dynamic modeling of dual-star permanent-magnet synchronous machines using look-up tables," in *2019 Electric Vehicles International Conference (EV)*. IEEE, 2019, pp. 1–6.
[13] Y. Hu, Z. Zhu, and M. Odavic, "Comparison of two-individual current control and vector space decomposition control for dual three-phase pmsm," *IEEE Transactions on Industry Applications*, vol. 53, no. 5, pp. 4483–4492, 2017.

VIII. Biographies

Abdolmajid Abedini Mohammadi received his B.Sc. and M.Sc. degrees in electrical engineering from Shahrekord University and Sharif University of Technology, both in Iran, in 2013 and 2015 respectively. From 2017 to 2018, he was an electrical engineer at the R&D department of Pars Generator Company, Tehran, Iran. He is currently with Brose Fahrzeugteile SE & Co. KG, Würzburg , Germany, within the Drives/Simulation Group as an Early-stage researcher (ESR) in the frame of the H2020 MSCA EID 2017-2021 research project INTERAC. Since 2018, he is a Ph.D. candidate at the BEAMS department of Université Libre de Bruxelles (ULB), Brussels, Belgium. His research interests are modeling, design, and control of electrical machines, and in particular of permanent-magnet synchronous machines.

Sebastian Ciceo obtained his M.Sc in Electrical Engineering from the Technical University of Cluj-Napoca in 2017. He currently works at Siemens PLM Software, Leuven as an Early-stage researcher (ESR) in the frame of the H2020 MSCA EID 2017-2021 research project INTERAC. He is pursuing a joint PhD degree with Université libre de Bruxelles and the Technical University of Cluj-Napoca. He's main research interest are: model-based system engineering and testing, electrical machines and drives, electrical mobility, structural dynamics, optimization and control.

Yves Mollet was born in Brussels, Belgium in 1987. He received the M.Eng. degree in electromechanical engineering from Haute Ecole Léonard de Vinci, in 2010 and the Ph.D. in engineering sciences and technology at the Université Libre de Bruxelles (ULB) in 2017. Both institutions are in Brussels, Belgium. He is currently a researcher at the ULB and at Siemens Industry Software, Leuven, Belgium. His main research topics concern fault detection and noise and vibrations in electrical machines and drives.

Adrian-Cornel Pop received the B.Sc. and M.Sc. degrees from the Technical University of Cluj-Napoca, Cluj-Napoca, Romania, in 2009 and 2010, respectively, both in electrical engineering, and the Ph.D. degree in the frame work of a joint program between the Technical University of Cluj-Napoca, and the Université Libre de Bruxelles, Brussels, Belgium, in 2012. He is first author or coauthor of some 20 scientific papers, 3 patents and one conference tutorial. He is currently with Brose Fahrzeugteile SE & Co. KG, Würzburg , Germany, within the Drives/Simulation Group. His current research is focused on optimal design for cost and performance of brushless AC and DC machines for automotive applications (i.e., power train, chassis, and thermal management) by means of multiphysics analysis starting from the customer-provided requirements and specifications. His past and current subjects of interest include design and optimization of electrical machines and drives (SRMs, PMSMs, and IMs), numerical methods, and hybrid and electrical vehicles.

Johan Gyselinck obtained his M.Sc. and PhD degree in electromechanical engineering from the Ghent University (Belgium) in 1991 and 2000 respectively. From 2000 till 2004 he was postdoctoral researcher and lecturer at the University of Liège (Belgium). Since 2004 he is professor at the Université Libre de Bruxelles (ULB, Belgium). His main teaching and research topics are low-frequency magnetics (finite-element and analytical modelling, numerical methods), electrical machines and drives (modelling, simulation, design and experimental work), and renewables (wind and photovoltaics). He is (co-)author of some 300 journal and conference papers.